Geophysical Research Letters

RESEARCH LETTER
10.1029/2019GL082437

The Impact of Mesoscale Gravity Waves on Homogeneous Ice Nucleation in Cirrus Clouds

B. Kärcher[1], E. J. Jensen[2], and U. Lohmann[3]

[1]DLR Oberpfaffenhofen, Institut für Physik der Atmosphäre, Wessling, Germany, [2]National Aeronautics and Space Administration, Ames Research Center, Mountain View, CA, USA, [3]ETH Zürich, Institute of Atmospheric and Climate Science, Zurich, Switzerland

Key Points:
- We present a systematic process study of effects of a spectrum of gravity waves on homogeneous ice nucleation in cirrus through ensemble simulations
- High cooling rates have disproportionately large impact on nucleated ice crystal number concentrations at low background updraft speeds
- Analysis of midlatitude continental cirrus measurements suggests impact of heterogeneous nucleation and sedimentation on total ice numbers

Supporting Information:
- Supporting Information S1

Correspondence to:
B. Kärcher,
bernd.kaercher@dlr.de

Citation:
Kärcher, B., Jensen, E. J., & Lohmann, U. (2019). The impact of mesoscale gravity waves on homogeneous ice nucleation in cirrus clouds. *Geophysical Research Letters*, *46*. https://doi.org/10.1029/2019GL082437

Received 12 FEB 2019
Accepted 22 APR 2019

Abstract Effects of a spectrum of mesoscale gravity waves on homogeneous aerosol freezing in midlatitude cirrus are studied by means of parcel model simulations that are driven by random vertical wind speeds constrained by balloon measurements. Stochastic wave forcing with mean updraft speeds of 5–20 cm/s leads to substantial nucleated ice crystal number concentrations (ICNC) of 0.1–1 cm^{-3} in situations with slow large-scale cooling, which by itself would generate fewer ice crystals. The stochastic nature of wave-driven air parcel temperatures enhances ICNC even further, but the times required to reach freezing conditions unsupported by large-scale cooling may vary widely. In the presence of wave forcing, ice crystals with low ICNC (<1–10 L^{-1}) are also generated by homogeneous freezing, albeit only rarely. Comparisons with aircraft measurements suggest significant influences of heterogeneous ice-nucleating particles and ice crystal sedimentation on ICNC, but quantifying their individual contributions remains elusive.

Plain Language Summary Spontaneous freezing of airborne, water-containing particles below −38 °C is a fundamental pathway to form ice crystals in high-altitude cirrus clouds. This ice formation process has been well researched and was the first represented in weather forecast and climate models to advance cirrus predictions. One key characteristic is its strong dependence of the number of ice crystals formed on the cooling rate of air. Recent observations show that rapid cooling rates are generated by ubiquitous gravity waves. Here, we explore the rich suite of phenomena taking place during cirrus formation caused by a spectrum of gravity waves. We find that wave effects should be considered in future model simulations, when comparing model results with observations, and in parameterizations of cloud ice crystal formation.

1. Introduction

Mesoscale air motion variability is crucial for the nucleation of ice crystals in cirrus (see Kärcher, 2017a, and references therein). We refer to cirrus as upper tropospheric ice clouds that form in situ, for example, in frontal systems. Superpressure balloon (SPB) measurements at altitudes of 18–21 km directly link mesoscale vertical wind speed and the associated temperature variability to gravity waves and quantified spectral properties (Podglajen et al., 2016; Schoeberl et al., 2017). Since these airborne measurement platforms are advected by the wind field, properties of fluctuations derived from them are highly useful for Lagrangian cloud studies. Dinh et al. (2016) and Jensen et al. (2016) used SPB temperature time series to drive detailed ice nucleation simulations, focussing on the tropical tropopause layer. Kienast-Sjögren et al. (2015)—using a Lagrangian microphysical aerosol-cloud model—investigated cirrus over a midlatitude site combining small-scale vertical wind speeds and temperature fluctuations inferred from radiosonde soundings and a high-resolution weather prediction model. Haag and Kärcher (2004) used results from a global weather prediction model with superimposed fluctuations to study hemispheric properties of midlatitude cirrus.

Mesoscale gravity waves are ubiquitous in the upper troposphere and lower stratosphere. SPB measurements show that power spectra of their properties versus intrinsic wave frequency are typically broad and continuous, consistent with a superposition of many waves. A spectrum of mesoscale gravity waves generates broad frequency distributions of ice crystal number concentrations (ICNC) via homogeneous freezing of supercooled aqueous solution particles (Hoyle et al., 2005; Jensen & Pfister, 2004; Kärcher & Ström, 2003).

The random nature of wave perturbations motivates the use of probabilistic methods to describe them. Process models have studied aspects of homogeneous freezing using randomized small-scale dynamical forcing (Dinh et al., 2016; Hoyle et al., 2005; Murphy, 2014; Shi & Liu, 2016).

Faithful applications of cirrus parameterizations in cloud schemes of large-scale models require sound representations of unresolved cooling rates (Lohmann & Kärcher, 2002). While the attribution of ice nucleation mechanisms in cirrus clouds in global climate models is challenging (Dietlicher et al., 2018; Gasparini et al., 2018) and such models have already begun to parameterize the impact of unresolved gravity waves on cirrus formation (Penner et al., 2018), it is important to explore this issue systematically on the process level as a prerequisite to improving ice nucleation parameterizations (Barahona & Nenes, 2008; Kärcher & Lohmann, 2002).

Before enhancing complexity by considering effects of heterogeneous ice-nucleating particles (INPs), which are poorly constrained by field observations at cirrus temperatures (<230–235 K; Hoose & Möhler, 2012; Jensen et al., 2018), we focus on the more basic and much better understood homogeneous freezing process. Field measurements leave little doubt that homogeneous freezing of supercooled aerosol particles is active in cirrus and responsible for at least the generation of the rightmost tail (>0.5 cm^{-3}) of probability distributions of ICNC. The main factor limiting INP effects is their low upper tropospheric number concentration (<0.1 cm^{-3}; DeMott et al., 2010), which makes them inefficient in suppressing homogeneous freezing in the presence of sufficiently large vertical wind speeds (DeMott et al., 1997). Nonetheless, potent INPs are capable of modulating or, if sufficiently abundant, dominating cirrus properties according to global model simulations (Gettelman et al., 2012; Kuebbeler et al., 2014; Penner et al., 2018; Shi & Liu, 2016; Zhou & Penner, 2014).

We explore systematically the homogeneous freezing process in midlatitude cirrus clouds due to gravity wave-driven fluctuations of vertical wind speed consistent with Lagrangian SPB measurements. The prescribed wave perturbations represent conditions away from strong local wave sources such as elevated mountain ridges or deep convective clouds. We evaluate statistically microphysical parcel model simulations forced with a large number of different random realizations of fluctuation time series. We compare our results with data taken during an extensive airborne field campaign, allowing us to extend previous findings on factors controlling midlatitude cirrus cloud formation (Jensen et al., 2013). We describe the stochastic ice nucleation simulations in section 2, analyze the results of tens of thousands of them and compare them to aircraft observations in section 3, and conclude our work in section 4.

2. Stochastic Simulations

The spectral parcel model *prime*ICE solves a large set of equations governing the temporal evolution of heat, water vapor, and supercooled/frozen water during ice nucleation and aqueous aerosol particle and ice crystal growth due to uptake of water vapor (Kärcher, 2017b). We consider ambient conditions above ice but below water saturation, where ice crystals can form homogeneously by freezing of liquid solution droplets.

Air parcel temperature, T, is adiabatically perturbed by random vertical wind speed fluctuations, w'. These fluctuations are superimposed onto a constant updraft speed, $w_0 \geq 0$, driving ice microphysics in the absence of wave-driven variability. Its prescribed value may be thought of as representative for synoptic conditions ($w_0 < 10$ cm/s), orographic forcing (10–100 cm/s and sometimes exceeding 1 m/s), or perturbations induced by convection (>1 m/s). Values of w_0 greater than 1–10 m/s are found in the detrainment zones of deep convective clouds, where homogeneous ice formation involves aerosol particles that have been activated into cloud droplets prior to or along with freezing at temperatures 233–238 K. Presumably, at these conditions, vertical wind speed fluctuations have different statistical properties (e.g., mean values, variances, and power spectral densities) than those caused by gravity waves, so the findings reported here are not directly applicable to such cases. Background wind speeds of (fractions of) millimeters per second are found in the tropical tropopause layer, where T is lower (<200 K) than in midlatitudes studied here.

A decomposition of updraft speeds has also been employed by Spichtinger and Krämer (2013), representing fluctuations by a monochromatic sinusodial wave. Investigating the impact of wave phase at which ice nucleation sets in, Jensen et al. (2010) showed that a spectrum of waves with random phases leads to broad ICNC distributions. Since the constant updraft w_0 introduced here refers to the large-scale vertical wind speeds resolved in global models, only the range $w_0 <$ 1–10 c/s is relevant. For higher w_0 values, the separa-

tion between constant updraft and wave-driven vertical wind speed fluctuations, w', is somewhat artificial. Outside of convection, waves are the only source of updraft speeds in excess of ≈10 cm/s and even smaller values associated with synoptic and planetary waves.

The wave forcing employed here accounts for the observed, double exponential (Laplacian) shape of the vertical wind speed statistic, $L(w') = \exp(-|w'|/\mu_w)/(2\mu_w)$. This distribution has zero mean, and μ_w is the mean value taken over the one-sided (updraft) statistic, relating to the standard deviation, σ_w, via $\mu_w \equiv 2\int_0^\infty w' L(w')dw' = \sigma_w/\sqrt{2}$. The Laplacian approximately fits Lagrangian measurements (Podglajen et al., 2016) and is used to generate fluctuation time series, $w'(t)$, one for each nucleation simulation. The vertical wind speed fluctuations are autocorrelated over a time $t_c = 2.8$ min. Therefore, they are defined only at discrete times (multiples of t_c) and were approximated by stair steps for numerical integration. The power spectrum of w' is flat (Figure 1 in Podglajen et al., 2016), meaning that all wave frequencies up to the Brunt-Väisälä frequency—an upper limit constraining gravity wave propagation—are included in the forcing with equal weight.

The temperature fluctuations, T', that result from the wind forcing are obtained by advancing the stochastic differential equation $DT'/Dt = -\Gamma w'$, where D/Dt denotes the Lagrangian (material) time derivative and $\Gamma \approx 0.01$ K/m is the dry adiabatic lapse rate. Individual w' values are sampled randomly from a Laplacian with prescribed standard deviation σ_w, or, in terms of adiabatic cooling rates (κ), $\sigma_\kappa = \Gamma\sigma_w$. This approach replicates the first-order autoregressive model to represent $T'(t)$ as proposed by Podglajen et al. (2016) based on the underlying w' measurements. In *prime*ICE, DT'/Dt is added to adiabatic and diabatic temperature tendencies, related to w_0 and latent heat exchange, respectively. Based on previous observational evidence, we choose a cooling rate standard deviation $\sigma_\kappa = 5$ K/hr as a baseline value at cirrus levels. Cooling rate fluctuations do not vary significantly with altitude within few kilometers around the tropopause (Podglajen et al., 2016).

Figure 1 shows results from parcel model simulations, each initialized at $T_0 = 221$ K (air pressure 300 hPa) and ice saturation ratio $S_0 = 1.3$. These values are slightly above (≈3 K for T_0) and below (≈0.2 for S_0) the values at freezing and were chosen such that mesoscale temperature variations are capable of triggering homogeneous freezing and within reasonable time scales (few hours). The initial total number density, mean dry radius, and geometric standard deviation of lognormally distributed aerosol particles were 500 cm^{-3}, 20 nm, and 1.5, respectively. We do not vary aerosol parameters, because the dependence of n on them is much weaker than on w (Kärcher & Lohmann, 2002; Kay & Wood, 2008; Liu & Shi, 2018). Time steps used in the simulations are variable, $\delta t\,[\mathrm{s}] = 1/(w_0 + |w'|)\,[cm/s]$, resolving individual freezing events. In addition, we imposed t_c as an upper limit time step to capture each vertical wind speed fluctuation.

With n indicating the number concentration of nucleated ice crystals, the circles in Figure 1 represent all $\{n, w_0\}$ data points resulting from an ensemble of 10,000 simulations. Each simulation was started with a random choice for w_0 and a different $w'(t)$-realization (given $\sigma_\kappa = 5$ K/hr or $\mu_w \approx 10$ cm/s) and terminated once the nucleated ice crystal number mixing ratio assumed a constant value after the first freezing event. The quenching of supersaturation right after freezing makes subsequent nucleation events unlikely, except in cases with very low n; therefore, the restriction of our analysis to first nucleation events is not problematic. Statistics of first freezing times are presented in the supporting information.

The simulations capture the dependence of nucleated ICNC on the homogeneous freezing temperature, $T_\star$, which is, however, very weak. We note that across all the cases discussed here, $T_* \approx 218$ K with very little scatter (±0.25 K), corresponding to a narrow range of ice saturation ratios, $S_\star \approx 1.5 \pm 0.02$, characteristic for homogeneous freezing events (Kärcher & Jensen, 2017). Examining the full upper tropospheric temperature range would reveal significant variations of $T_\star$ and nucleated ICNC.

The data points in Figure 1 exhibit considerable scatter for $w_0 < 10$–20 cm/s, about 15% lie below $n = 10^{-3}$ cm^{-3}. These nonpersistent cooling events have been termed temperature limited by Dinh et al. (2016). Most of these low-n events are generated when w' changes its sign before the freezing event is completed. They happen to occur since the wave-driven vertical wind speed fluctuations contain high-frequency contributions associated with time scales of 5–10 min, comparable to the duration of homogeneous freezing events (minutes; Jensen et al., 2016). The fraction of nonpersistent cooling events would be lower without restricting the analysis to first freezing times.

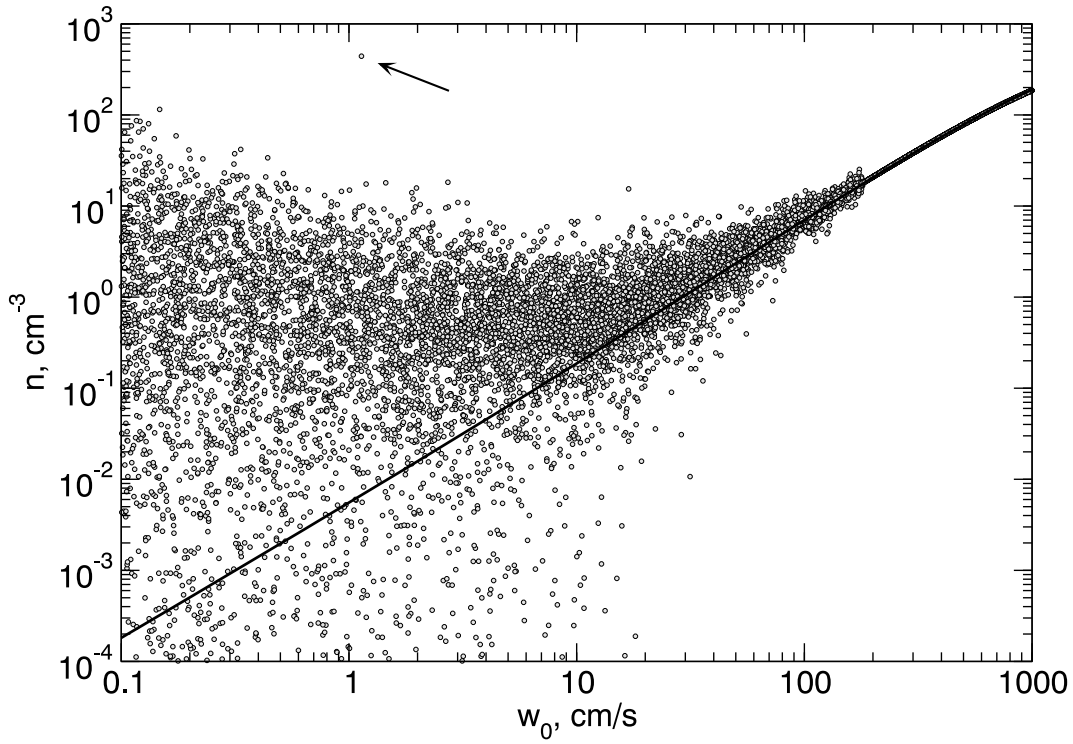

Figure 1. Number concentration, n, of homogeneously nucleated ice crystals versus background updraft speed, w_0, from ensemble simulations (circles). In each case, gravity wave-induced vertical wind speed fluctuations driving ice microphysics in the parcel simulations were randomly sampled from a Laplacian distribution with a mean value of updraft speed (standard deviation of cooling rate) fluctuations $\mu_w = 10$ cm/s ($\sigma_{\kappa\approx}5$ K/hr) added to the constant w_0. The arrow points to an excessively high concentration generated by an exceptionally large updraft fluctuation. The curve was obtained from simulations without fluctuations.

The scatter of n in a given narrow w_0-range decreases progressively with increasing w_0. The curve obtained from simulations without fluctuations follows a power law dependence, as expected from cloud physical theory (Kärcher & Lohmann, 2002): $n(w) = n_1 [(w_0 + w')/w_1]^\alpha$, where n_1 is the nucleated ICNC at a given T and $w = w_1$. A good fit at $T = 218$ K is obtained for $n_1 = 0.185\,\mathrm{cm}^{-3}$, $w_1 = 10$ cm/s, and $\alpha = 3/2$ (Figure 1). The data collapse onto this curve beyond $w_0 = 1$ m/s, showing that w_0 governs ice formation for $w_0 \gg \mu_w$ (deterministic regime). By contrast, ice formation is entirely controlled by the fluctuations for $w_0 \ll \mu_w$ (fluctuation-dominated regime). In the deterministic regime, nonpersistent cooling events no longer occur; we do not discuss this regime any further with $\mu_w = 5 - 20$ cm/s, as we are concerned with nonconvective (in situ) ice formation, where values $w_0 < 10$ cm/s prevail.

The arrow highlights a very rare data point indicating ≈400 ice crystals per cubic centimeter of air. In this case, one single freezing event caused by an updraft speed fluctuation of 16.7 m/s ($\approx 10\,\sigma_w$) depleted about 80% of the available aerosol particles. Fluctuation amplitudes of comparable magnitude are captured by the non-Gaussian statistic, $L(w')$. The probability of occurrence of such a value is $\exp(-10\sqrt{2}) \approx 10^{-6}$. This means that in a sample of 10,000 data points, there is a ≈1% chance of encountering such an event. Filling the gap between the outlier and the majority of the other data points in Figure 1 requires a much larger number of simulations.

3. Analysis of Nucleated ICNC

3.1. Expectation Values

We performed two additional sets of simulations halving and doubling the mean vertical wind forcing of 10 cm/s. We calculated in each case moving averages of n over 75 w_0 data points from the full $\{n, w_0\}$ data sets. Figure 2 shows the resulting averaged ICNC, $\mu_n(w_0)$ (expectation values). As expected from the above, the nucleated concentrations converge showing decreasing scatter as w_0 enters the deterministic regime.

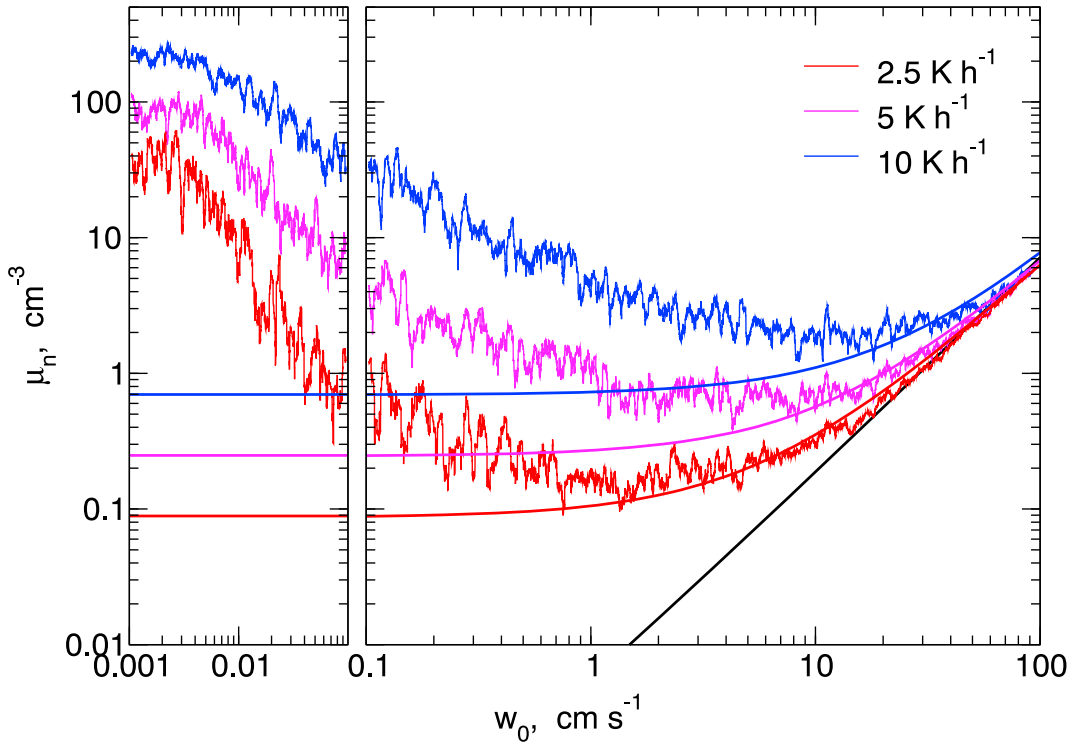

Figure 2. Mean ice crystal number concentration, μ_n, versus w_0 from ensemble simulations for three cases $\sigma_\kappa = 2.5, 5, 10$ K/hr (red, magenta, and blue), or $\mu_w \approx 5, 10, 20$ cm/s ($\sigma_w \approx 7.5, 15, 30$ cm/s, respectively. The black curve is obtained from simulations without fluctuations, where ice forms at w_0. For comparison, the colored smooth curves mark the mean nucleated concentrations calculated analytically from the updraft speed statistic. The left panel highlights the transition of simulated μ_n to vanishing background cooling ($w_0 \to 0$).

A surprising feature is the increase of μ_n for low w_0 that is most pronounced for larger forcing. We would expect the nucleated ICNC to approach a constant value for $w_0 \ll \mu_w$, if we just looked at the mean ICNC calculated directly from the updraft speed fluctuation statistic without accounting for sink processes of the ICNC. We call those values—shown as smooth colored curves in Figure 2—instantaneous ice numbers (equation (S4)).

High cooling rates have a greater chance than low cooling rates to reach freezing thresholds, $\{T_\star, S_\star\}$, giving them a large statistical weight despite their lower abundance in the updraft distribution. For example, at T already close close to $T_\star$, while a small cooling rate might not suffice to reach $T_\star$, a high cooling rate might well trigger freezing. This effect (coined preferential freezing) is stronger the larger μ_w and significantly increases μ_n as w_0 diminishes. With increasing w_0 pushing the parcel faster close to freezing conditions, low cooling rate fluctuations have an increasing chance to nucleate ice as well. The contribution of the fluctuations to w is dwarfed by w_0 for $w_0 \gg \mu_w$.

This said, we still expect μ_n to saturate in the limit $w_0 \to 0$, at which point the air parcels undergo a pure random temperature (supersaturation) walk unsupported by a constant baseline cooling. The left panel in Figure 2 extends the simulations to lower w_0 and indeed shows the expected behavior as $w_0 \to 0$. An immediate implication is that freezing is also possible for slightly negative w_0 causing a background warming. However, stronger subsidence will make cirrus formation increasingly unlikely due to the rapidly growing separation between the diminishing ice supersaturation and the homogeneous freezing threshold.

Preferential freezing results from the stochastic nature of the temperature fluctuations. It is absent in estimates of instantaneous values of nucleated ICNC (colored curves), or when the updraft statistic is equal to, or approaches, a monodisperse distribution. Apart from this, preferential freezing does not depend on the exact functional form of w' statistic, as long as it has a finite second moment. Times at which freezing conditions are met along a stochastic air parcel trajectory vary widely depending on the actual mesoscale temperature evolution and hence on how far initial conditions $\{S_0, T_0\}$ are away from $\{S_\star, T_\star\}$ (Figure S3). These times

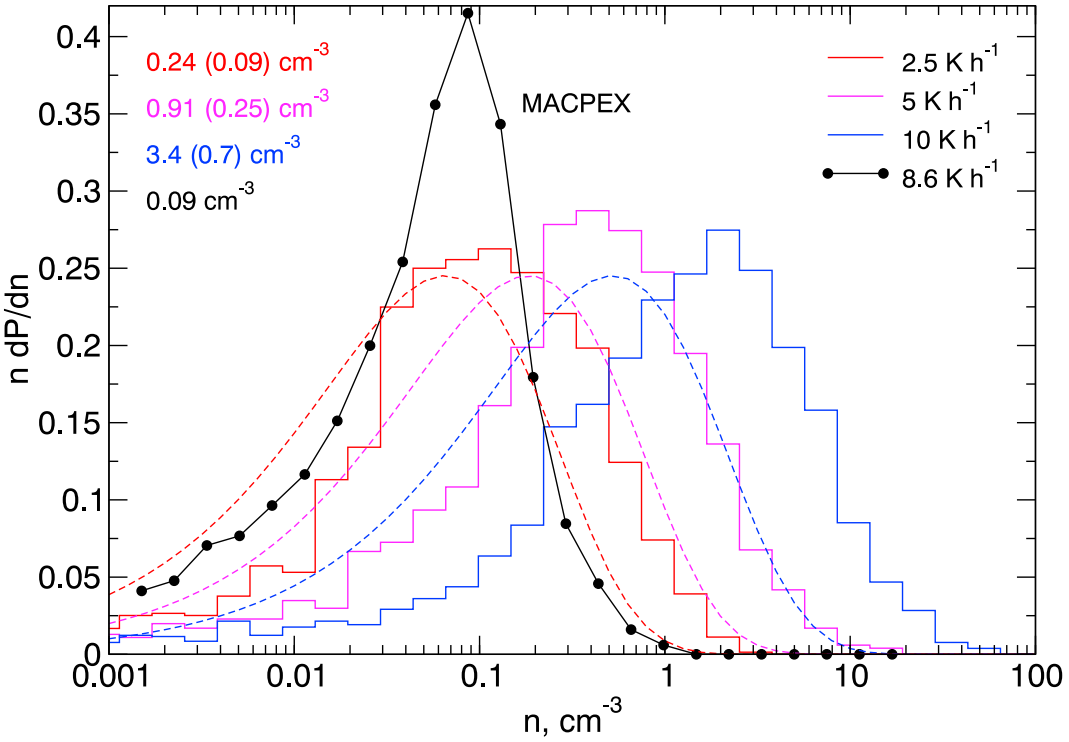

Figure 3. Probability of occurrence of the number concentration, n, of homogeneously frozen ice crystals for the color-coded cases shown in Figure 2. The simulation results (stair steps) with homogeneous freezing temperatures near 218 K include the effect of preferential freezing. We include the instantaneous statistics without preferential freezing (dashed curves) for each simulation case. Both stochastic and deterministic distributions are compared to the statistic (black curve) derived from aircraft measurements of midlatitude cirrus (Midlatitude Cirrus Properties Experiment [MACPEX]). Total nucleated number concentrations of ice crystals with all sizes (typically > 1 μm), averaged over 1 cm/s $\leq w_0 \leq \mu_w$ in each simulation case (or calculated analytically from the instantaneous statistics) and from MACPEX for ice crystal sizes > 15μm taken in the temperature range 215–221 K, are given in the left legend.

may take values comparable to, or longer than, the times over which w_0, S_0, and T_0 change in the atmosphere. If S_0 (T_0) is low (high) enough, mesoscale temperature variations by themselves may not meet homogeneous freezing conditions. Therefore, the high mean ICNC approached in the fluctuation-dominated regime may not be realized to the same extent in the atmosphere.

3.2. Comparison With Observations

Normalized probability density functions, dP/dn, represent the fraction of n values that fall into a given number density bin. The related distribution, $n\,dP/dn$, measures the probability of occurrence of given n values. The area under the latter is equal to the total ICNC. In Figure 3, we compare simulation results for $n\,dP/dn$ and instantaneous statistics that do not account for preferential freezing (equation (S7)) with data taken during the Midlatitude Cirrus Properties Experiment (MACPEX), an airborne field campaign that focused on synoptically forced midlatitude cirrus clouds over the south central United States (Jensen et al., 2013). The vertical wind speed measurements showed exponential updraft speed statistics with large flight-to-flight variability of mean updraft speeds. Mean values in nonconvective situations were in the range 13–21 cm/s (on average 17 cm/s), corresponding to $\sigma_\kappa = 6.6 - 10.6$ K/hr (on average 8.6 K/hr).

The simulated ICNC statistics were averaged across the fluctuation-dominated regime within 1 cm/s $\leq w_0 \leq \mu_w$; values $w_0 < 1$ cm/s are unlikely to be significant for synoptically forced midlatitude cirrus. We note that the range of w_0 over which the simulated distributions need to be averaged to allow for a fair comparison with the measurements is not well constrained. The MACPEX data set contains no information on the age of ice crystals past nucleation, preventing us from constraining the data to freshly nucleated ice crystals.

The peak regions of the simulated statistics shift to the right as the underlying cooling rates increase, indicating an increase in total nucleated ICNC. The statistics contain relatively few nonpersistent cooling events in their flat leftmost tails ($n < 0.01$ cm^{-3}), which are therefore of minor importance for the mean

nucleated ICNC. Otherwise, the overall shape of the simulated statistics is similar to the instantaneous distributions, reinforcing the current understanding that wave-driven vertical wind speed variability and homogeneous freezing are important contributors to ice formation in cirrus (Hoyle et al., 2005; Shi & Liu, 2016). Instantaneous and stochastic results differ more in terms of total ICNC with greater forcing.

The observed distribution is narrower than the simulated ones and has lower total ICNC. We expect differences between these distributions, since the MACPEX data contain ICNCs sampled at various stages of the cirrus cloud, while the parcel simulations only consider nucleated ice crystals. Moreover, the ICNC data used to generate the MACPEX statistic only include ice crystals with sizes larger than 15 μm. Uncertainty associated with the first size bin of the measurements precludes useful quantitative information about the concentration of the smallest ice crystals. The sizes of simulated ice crystals, and hence their fall speeds, are typically smaller than 15 μm after quenching the initially high supersaturation (Kärcher & Lohmann, 2002).

Regarding differences in shape, we note that the left (low-n) wing of the observed distribution might be affected by sample volume limitations of the measurements. Therefore, it is not possible to fully capture nonpersistent cooling events to the degree they are present in the data set in the first place. Preferential freezing, which increases total ICNC in the stochastic simulations relative to the instantaneous values, might not occur in nature to the same extent as simulated. This is possible, since the simulations allow for a very large number of trajectories each with virtually unrestricted time to allow nucleation to be triggered, while in a real cirrus cloud time for freezing events to take place is affected by larger-scale wave activity changing w_0 on short periods of time. The right wing of the observed distribution decays faster than the simulations indicated. It is possible that high-n events are underrepresented in the data set, since they happen to be rather localized and more easily missed by the probing aircraft (Jensen et al., 2013). We note that the MACPEX statistic contains very few ICNC data >10 cm^{-3}, consistent with homogeneous freezing triggered by $w' > 1.4$ m/s.

More importantly, given the rather vigorous mean cooling rate prevailing during MACPEX ($\sigma_\kappa = 8.6$ K/hr), the total ice crystal number is low (0.09 cm^{-3}). The instantaneous statistic that disregards enhancements in ICNC due to preferential freezing yields the same total ICNC as MACPEX only when evaluated at $\sigma_\kappa = 2.5$ K/hr. If we compute the total ICNC directly from instantaneous expectation values, we obtain $\mu_n = 0.09$–0.7 cm^{-3} from equation (S8) (see also Figure 2) for the range of mean updraft speeds prevailing during MACPEX. Even this estimate is one to eight times higher than the measurements indicate.

We offer two explanations to account for the discrepancy in total nucleated ICNC, which is not entirely unexpected. On the one hand, ice crystal sedimentation may reduce total ICNC significantly in midlatitude cirrus, in which a relatively large amount of water vapor available for growth produces ice crystals with large fall speeds. Quantification of this effect requires at least a one-dimensional model treatment. On the other hand, we know that ice crystals present before homogeneous freezing commences either cause lower homogeneously nucleated ICNC or suppress homogeneous freezing altogether. This happens because preexisting ice crystals act as a sink for water vapor, exerting an effect on nucleated ICNC that may be accounted for by introducing a fictitious downdraft (Kärcher et al., 2006). This downdraft basically offsets part of the mean updraft speed of the fluctuations applied in our simulations.

Preexisting ice in a nucleating air parcel could be generated in a past ice formation event, possibly by active INP. DeMott et al. (1997) estimated with parcel model simulations a maximum impact of INP on cirrus formation for updraft speeds <20 cm/s, suggesting the potential importance of INP in wave-driven scenarios. During MACPEX, the lower troposphere was polluted, and deep convection was frequently occurring. It is therefore reasonable to assume that INP were available at cirrus levels, consistent with a study that showed that some aerosol types were enhanced in ice residuals compared to ambient (interstitial) aerosols (Cziczo et al., 2013). However, this study did not quantify the balance between heterogeneous and homogeneous nucleation in midlatitude cirrus. Without specific knowledge of number concentrations and physico-chemical properties of INP, we cannot conclusively assess the role of heterogeneous ice nucleation in affecting the relationship between total nucleated ICNC and mean updraft speed fluctuation.

4. Conclusions and Outlook

In an attempt to contribute to a fundamental understanding of processes governing the formation of ice clouds, we study effects of a spectrum of ever-present mesoscale gravity waves on homogeneous aerosol

freezing in midlatitude cirrus. The dynamical forcing due to vertical wind speeds (causing adiabatic temperature fluctuations) is parameterized based on direct Lagrangian measurements constraining a comprehensive microphysical parcel model. The random forcing does not represent the effect of strong updrafts induced by localized high-frequency (orographic or convective) gravity wave sources. Results of stochastic simulations of cirrus formation differ in important ways from traditional deterministic results used in data-model comparison exercises and for parameterization development.

We find that high updraft speed fluctuations increase total nucleated ICNC to much larger values than those calculated deterministically based solely on the probability of occurrence of the fluctuations. This preferential freezing effect is a consequence of the stochastic nature of wave-driven temperature fluctuations. It occurs in low mean wind conditions and whenever a nonnegligible number of high updraft speeds populates the wing of the wave forcing statistic; it may be suppressed in the presence of efficient INP. Given the rather long times required for stochastic trajectories to trigger freezing even in air that is already ice supersaturated, future studies should investigate in which situations large-scale cooling, local relative humidity, and INP conditions are most relevant for atmospheric applications.

In the current stochastic model, asymptotic temperature fluctuation variance across an ensemble of fluctuation time series increases linearly over time. In better agreement with observations, inclusion of a low-frequency damping to the temperature fluctuations would lead to a stationary variance, reminiscent of Brownian motion (Landau & Lifshitz, 1987). While the effect of such damping is unimportant for the present study, its effect on first freezing times for less ice supersaturated initial conditions and weak or absent large-scale forcing should be studied in future work.

We confirm that rapid sign reversal of vertical wind speeds during freezing events causes only few ($<$1–10 L^{-1}) ice crystals to form. We show that these nonpersistent cooling events are rare occurring less than 15% of the time in the conditions of this study; they affect the total nucleated ICNC only to a small degree in the midlatitude conditions studied here. For specific applications, it might be useful to explore how this fraction changes in other meteorological situations.

We simulate probability distributions of nucleated ICNC and compare them with those calculated analytically from the distribution of the updraft speed forcing. The overall similarity of the shapes of simulated and analytical statistics suggests that wave-driven dynamical forcing and homogeneous freezing play important roles in in situ cirrus formation, inasmuch as ICNC values $>10\,cm^{-3}$ have been measured in cirrus. Such high concentrations, although detected only rarely, are difficult to explain otherwise.

More importantly, differences between measured and simulated ICNC statistics are consistent with the potential importance of ice crystal sedimentation and INP in cirrus as observed during an aircraft campaign over the continental United States. We have designed the model setup such that differences between the results and these observations were expected rather than to explain the measurements. Given mean updraft speeds of 17 cm/s during the measurements, relatively low mean ICNC (90 L^{-1}) with sizes $>15\,\mu m$ have been reported in the temperature range 215–221 K, but many more are predicted (including ice crystals with smaller sizes). Lack of information about INP number concentrations and their properties preclude robust quantification of their impact. Moreover, the relative roles of INP and sedimentation as potential causes for low total nucleated ICNC despite strong wave forcing are difficult to disentangle given the limited data set and the restrictions of a parcel model framework.

Our methodology sets the scene for more comprehensive cirrus simulations with at least vertical spatial resolution including ice crystal sedimentation, heterogeneous ice nucleation, and gravity wave forcing. Consideration of these processes enables more realistic estimations of how INP modify cirrus formation processes and more realistic data-model comparisons of nucleated ICNC. Besides measuring meteorological and INP-relevant data, future cirrus measurements should characterize cloud particle variables along with the small-scale vertical wind fields in which cirrus form. On the modeling side, an ambitious goal is the development of a full three-dimensional model that includes effects of shear, mixing, and radiative flux changes and at the same time resolves the high-frequency gravity waves and includes their impacts on cirrus formation and evolution.

Our findings have important implications for the representation of cirrus in global models. Most ice nucleation parameterizations are based on an idealized treatment of updraft speeds. When including the effects of waves, geographical, seasonal, and topographic variability in updraft speeds should be accounted for.

Moreover, wave-generated enhancements of ICNC in the fluctuation-dominated regime should be properly parameterized. Inclusion of stochastic effects warrants careful consideration by considering differences between first freezing times and time steps used in large-scale models. We also encourage the coupling of cirrus parameterizations with a treatment of the subsequent sedimentation effect on nucleated ICNC. This will be particularly important if these parameterizations describe competing effects between INP and supercooled liquid aerosol particles during ice formation.

Acknowledgments
Data used in this study is available at https://espoarchive.nasa.gov/.

References

Barahona, D., & Nenes, A. (2008). Parameterization of cirrus cloud formation in large-scale models: Homogeneous nucleation. *Journal of Geophysical Research*, *113*, D11211. https://doi.org/10.1029/2007JD009355

Cziczo, D. J., Froyd, K. D., Hoose, C., Jensen, E. J., Diao, M., Zondlo, M. A., et al. (2013). Clarifying the dominant sources and mechanisms of cirrus cloud formation. *Science*, *357*, 6138. https://doi.org/10.1126/science.1234145

DeMott, P. J., Prenni, A. J., Liu, X., Kreidenweis, S. M., Petters, M. D., Twohy, C. H., et al. (2010). Predicting global atmospheric ice nuclei distributions and their impacts on climate. *Proceedings of the National Academy of Sciences of the United States of America*, *107*, 11,217–11,222.

DeMott, P. J., Rogers, D. C., & Kreidenweis, S. M. (1997). The susceptibility of ice formation in upper tropospheric clouds to insoluble aerosol components. *Journal of Geophysical Research*, *102*, 19,575–19,584.

Dietlicher, R., Neubauer, D., & Lohmann, U. (2018). Elucidating ice formation pathways in the aerosol-climate model ECHAM6-HAM2. *Atmospheric Chemistry and Physics, Discussions*, *18*. https://doi.org/10.5194/acp-2018-573

Dinh, T., Podglajen, A., Hertzog, A., Legras, B., & Plougonven, R. (2016). Effect of gravity wave temperature fluctuations on homogeneous ice nucleation in the tropical tropopause layer. *Atmospheric Chemistry and Physics*, *16*, 35–46.

Gasparini, B., Meyer, A., Neubauer, D., Münch, S., & Lohmann, U. (2018). Cirrus cloud properties as seen by the CALIPSO satellite and ECHAM-HAM global climate model. *Journal of Climate*, *31*, 1983–2003.

Gettelman, A., Liu, X., Barahona, D., Lohmann, U., & Chen, C. (2012). Climate impacts of ice nucleation. *Journal of Geophysical Research*, *117*, D20201. https://doi.org/10.1029/2012JD017950

Haag, W., & Kärcher, B. (2004). The impact of aerosols and gravity waves on cirrus clouds at midlatitudes. *Journal of Geophysical Research*, *109*, D12202. https://doi.org/10.1029/2004JD004579

Hoose, C., & Möhler, O. (2012). Heterogeneous ice nucleation on atmospheric aerosols: A review of results from laboratory experiments. *Atmospheric Chemistry and Physics*, *12*, 9817–9854.

Hoyle, C. R., Luo, B. P., & Peter, Th. (2005). The origin of high ice crystal number densities in cirrus clouds. *Journal of the Atmospheric Sciences*, *62*, 2568–2579.

Jensen, E. J., Kärcher, B., Ueyama, R., Pfister, L., Bui, T. V., Diskin, G. S., et al. (2018). Heterogeneous ice nucleation in the tropical tropopause layer. *Journal of Geophysical Research: Atmospheres*, *123*, 12,210–12,227. https://doi.org/10.1029/2018JD028949

Jensen, E. J., Lawson, R. P., Bergman, J. W., Pfister, L., Bui, T. P., & Schmitt, C. G. (2013). Physical processes controlling ice concentrations in synoptically-forced, midlatitude cirrus. *Journal of Geophysical Research: Atmospheres*, *118*, 5348–5360. https://doi.org/10.1002/jgrd.50421

Jensen, E. J., & Pfister, L. (2004). Transport and freeze-drying in the tropical tropopause layer. *Journal of Geophysical Research*, *109*, D02207. https://doi.org/10.1029/2003JD004022

Jensen, E. J., Pfister, L., Bui, T. P., Lawson, R. P., & Baumgardner, D. (2010). Ice nucleation and cloud microphysical properties in tropical tropopause layer cirrus. *Atmospheric Chemistry and Physics*, *10*, 1369–1384.

Jensen, E. J., Ueyama, R., Pfister, L., Bui, T. P., Alexander, M. J., Podglajen, A., et al. (2016). High-frequency gravity waves and homogeneous ice nucleation in tropical tropopause layer cirrus. *Geophysical Research Letters*, *43*, 6629–6635.

Kärcher, B. (2017a). Cirrus clouds and their response to anthropogenic activities. *Current Climate Change Reports*, *3*, 45–57. https://doi.org/10.1007/s40641-017-0060-3

Kärcher, B. (2017b). Homogeneous ice formation in convective cloud outflow regions. *Quarterly Journal of the Royal Meteorological Society*, *143*, 2093–2103. https://doi.org/10.1002/qj.3069

Kärcher, B., Hendricks, J., & Lohmann, U. (2006). Physically based parameterization of cirrus cloud formation for use in global atmospheric models. *Journal of Geophysical Research*, *111*, D01205. https://doi.org/10.1029/2005JD006219

Kärcher, B., & Jensen, E. J. (2017). Microscale characteristics of homogeneous freezing events in cirrus clouds. *Geophysical Research Letters*, *44*, 2027–2034. https://doi.org/10.1002/2016GL072486

Kärcher, B., & Lohmann, U. (2002). A Parameterization of cirrus cloud formation: Homogeneous freezing including effects of aerosol size. *Journal of Geophysical Research*, *107*, 4164. https://doi.org/10.1029/2001JD000429

Kärcher, B., & Ström, J. (2003). The roles of dynamical variability and aerosols in cirrus cloud formation. *Atmospheric Chemistry and Physics*, *3*, 823–838.

Kay, J. E., & Wood, R. (2008). Timescale analysis of aerosol sensitivity during homogeneous freezing and implications for upper tropospheric water vapor budgets. *Geophysical Research Letters*, *35*, L10809. https://doi.org/10.1002/2007GL032628

Kienast-Sjögren, E., Miltenberger, A. K., Luo, B. P., & Peter, Th (2015). Sensitivities of Lagrangian modelling of mid-latitude cirrus clouds to trajectory data quality. *Atmospheric Chemistry and Physics*, *15*, 7429–7447.

Kuebbeler, M., Lohmann, U., Hendricks, J., & Kärcher, B. (2014). Dust ice nuclei effects on cirrus clouds. *Atmospheric Chemistry and Physics*, *14*, 3027–3046.

Landau, L. D., & Lifshitz, E. M. (1987). *Course of Theoretical Physics* (Vol. 5). Butterworth-Heinemann: Statistical Physics.

Liu, X., & Shi, X. (2018). Sensitivity of homogeneous ice nucleation to aerosol perturbations and its implications for aerosol indirect effects through cirrus clouds. *Geophysical Research Letters*, *45*, 1684–1691. https://doi.org/10.1002/2017GL076721

Lohmann, U., & Kärcher, B. (2002). First interactive simulations of cirrus clouds formed by homogeneous freezing in the ECHAM general circulation model. *Journal of Geophysical Research*, *107*, 4105. https://doi.org/10.1029/2001JD000767

Murphy, D. M. (2014). Rare temperature histories and cirrus ice number density in a parcel and a one-dimensional model. *Atmospheric Chemistry and Physics*, *14*, 13,013–13,022.

Penner, J. E., Zhou, C., Garnier, A., & Mitchell, D. L. (2018). Anthropogenic aerosol indirect effects in cirrus clouds. *Journal of Geophysical Research: Atmospheres*, *123*, 11,652–11,677. https://doi.org/10.1002/2018JD029204

Podglajen, A., Hertzog, A., Plougonven, R., & Legras, B. (2016). Lagrangian temperature and vertical velocity fluctuations due to gravity waves in the lower stratosphere. *Geophysical Research Letters*, *43*, 3543–3553. https://doi.org/10.1002/2016GL068148

Schoeberl, M. R., Jensen, E., Podglajen, A., Coy, L., Lodha, C., Candido, S., & Carver, R. (2017). Gravity wave spectra in the lower stratosphere diagnosed from project Loon balloon trajectories. *Journal of Geophysical Research: Atmospheres*, *122*, 8517–8524. https://doi.org/10.1002/2017JD026471

Shi, X., & Liu, X. (2016). Effect of cloud-scale vertical velocity on the contribution of homogeneous nucleation to cirrus formation and radiative forcing. *Geophysical Research Letters*, *43*, 6588–6595. https://doi.org/10.1002/2016GL069531

Spichtinger, P., & Krämer, M. (2013). Tropical tropopause ice clouds: A dynamic approach to the mystery of low crystal numbers. *Atmospheric Chemistry and Physics*, *13*, 9801–9818.

Zhou, C., & Penner, J. E. (2014). Aircraft soot indirect effect on large-scale cirrus clouds: is the indirect forcing by aircraft soot positive or negative. *Journal of Geophysical Research: Atmospheres*, *119*, 11,303–11,320. https://doi.org/10.1002/2014JD021914

Supporting Information for

"The impact of mesoscale gravity waves on homogeneous ice nucleation in cirrus clouds"

B. Kärcher[1], E. J. Jensen[2], and U. Lohmann[3]

[1]DLR Oberpfaffenhofen, Institut für Physik der Atmosphäre, Wessling, Germany

[2]National Aeronautics and Space Administration, Ames Research Center, Moffett Field, CA, USA

[3]ETH Zürich, Institute of Atmospheric and Climate Science, Zurich, Switzerland

Instantaneous statistic and expectation value of nucleated ice crystal number concentration

We derive the instantaneous ice number statistic directly from that of updraft speed fluctuations. We begin by calculating analytically the mean (expected) number concentration, ICNC, of homogeneously nucleated ice crystals resulting from subjecting air parcels to a large number of vertical wind speed trajectories.

According to observations, the normalized probability density function (PDF) of updraft speed fluctuations, $w' \geq 0$, is given by

$$\frac{dP}{dw'} = \frac{1}{\mu_w} e^{-w'/\mu_w}\,, \tag{S1}$$

with the mean value, μ_w. The probability of finding updraft speed fluctuations exceeding $w_\star$ is given by $\int_{w_\star}^{\infty}(dP/dw')dw' = \exp(-w_\star/\mu_w)$.

According to cloud physical theory, the nucleated ICNC, $n(w)$, exhibits a power law dependence on the total vertical wind speed, $w = w_0 + w'$ ($w_0 \geq 0$ is a constant mean updraft speed):

$$n(w) = n_1\left(\frac{w}{w_1}\right)^{\alpha}, \quad w = w_0 + w'\,; \tag{S2}$$

The set of values $\{n_1, w_1\}$ is temperature-dependent.

The instantaneous expectation value of n, the nucleated ICNC calculated directly from the distribution of updraft speed fluctuations, follows from:

$$\mu_n = \int_0^{\infty} n(w_0 + w')\frac{dP}{dw'}dw'\,. \tag{S3}$$

Corresponding author: Bernd Kärcher, bernd.kaercher@dlr.de

Integrating Eq. (S3) yields:

$$\mu_n = n(w_0)F_\alpha(x)\,, \quad F_\alpha(x) = \frac{e^x}{x^\alpha}\Gamma(\alpha+1,x)\,, \quad x = \frac{w_0}{\mu_w}\,. \tag{S4}$$

The dimensionless parameter, x, connects fluctuation-dominated ($x \ll 1$) and deterministic regimes ($x \gg 1$). Recalling that $\alpha = 3/2$ and using the recurrence relation for the incomplete Gamma function, $\Gamma(\alpha+1,x) = \alpha\Gamma(\alpha,x)+x^\alpha e^{-x}$, twice along with $\Gamma(1/2,x) = \sqrt{\pi}\,\mathrm{erfc}(\sqrt{x})$ and the complementary error function, $\mathrm{erfc}(y) = 1-(2/\sqrt{\pi})\int_y^\infty e^{-t^2}dt$, we get:

$$F_{3/2}(x) = 1 + \frac{3}{2x} + \frac{3\sqrt{\pi}}{4x^{3/2}}\left\{e^x\mathrm{erfc}(\sqrt{x})\right\}. \tag{S5}$$

It is easy to show that μ_n has the asymptotic values: $F_{3/2}(x \gg 1) \to 1$ and therefore $\mu_n \to n(w_0)$; moreover, $F_{3/2}(x \ll 1) \to 3\sqrt{\pi}/(4x^{3/2})$ and therefore $\mu_n \to (3\sqrt{\pi}/4)\,n(\mu_w)$.

In the deterministic regime ($w_0 \gg \mu_w$), the fluctuations have little to no effect on μ_n. In the fluctuation-dominated regime ($w_0 \ll \mu_w$), (i) μ_n takes a constant value as μ_w is fixed; (ii) $n(\mu_w)$ is significantly larger than $n(w_0)$ due to the power law dependence $n \propto w^{3/2}$; and (iii) this value is further enhanced by the factor $(3\sqrt{\pi}/4) \approx 1.33$ due to the exponential shape of the w'-statistic. In Fig. S1, we show the relationship $x^{3/2}F_{3/2}(x)$.

We calculate the instantaneous PDF of nucleated ice numbers, ndP/dn, by evaluating

$$\frac{dP}{dn} = \frac{dP/dw'}{dn/dw'} \tag{S6}$$

applying Eqs. (S1)+(S2) in the fluctuation-dominated regime (setting $w_0 = 0$). The solution reads

$$z\frac{dP}{dz} = \gamma\, z^\gamma\, e^{-z^\gamma}\,, \quad \gamma = \frac{1}{\alpha}\,, \quad z = \frac{n}{n(\mu_w)}\,, \tag{S7}$$

and is depicted in Fig. S2. We may also compute the instantaneous mean nucleated ICNC as the area under this distribution:

$$\mu_n = n(\mu_w)\int_0^\infty x^\alpha\, e^{-x}dx = \Gamma(\alpha+1,0)\,n(\mu_w) \equiv \Gamma(5/2)\,n(\mu_w)\,, \tag{S8}$$

consistent with Eq. (S4) in the limit $x \to 0$. We note that the shape factor, $\Gamma(5/2) = 3\sqrt{\pi}/4$, converts to unity when Eq. (S1) is replaced by a delta distribution.

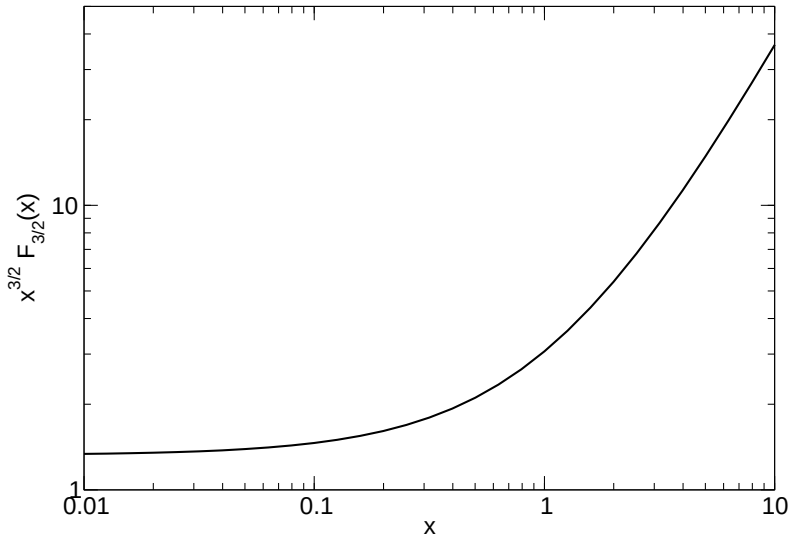

Figure S1. Scaled nucleated ice crystal number concentration calculated as an expectation value from an exponential distribution of updraft speed fluctuations as a function of the scaled mean updraft speed, $x=w_0/\mu_w$. In the limit $x\rightarrow 0$, the curve indicates the value of the shape parameter characterizing the updraft statistic, $\Gamma(5/2)\approx 1.33$.

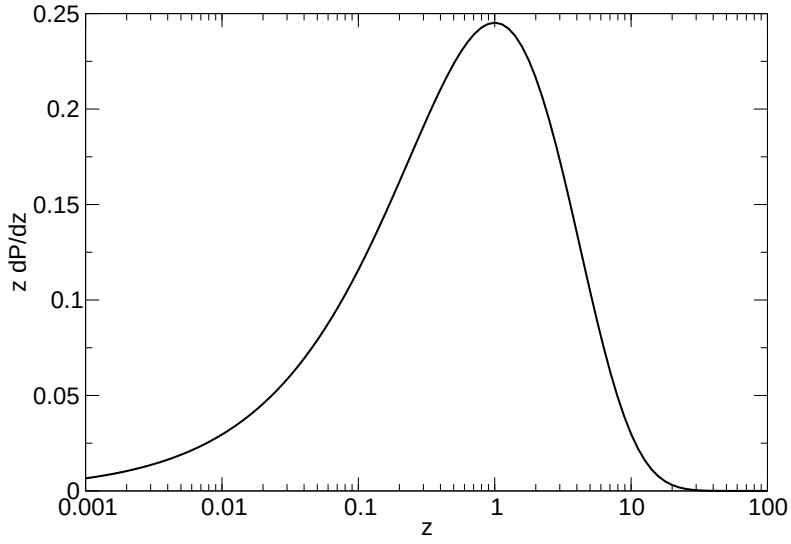

Figure S2. Probability density function of nucleated ice crystal number concentrations, zdP/dz, calculated from an exponential distribution of updraft speed fluctuations in the fluctuation-dominated regime and shown as a function of the similarity variable $z=n/n(\mu_w)$. Lowering (increasing) μ_w shifts the statistic to the left (right) without affecting its shape or maximum.

Statistic of first homogeneous freezing times

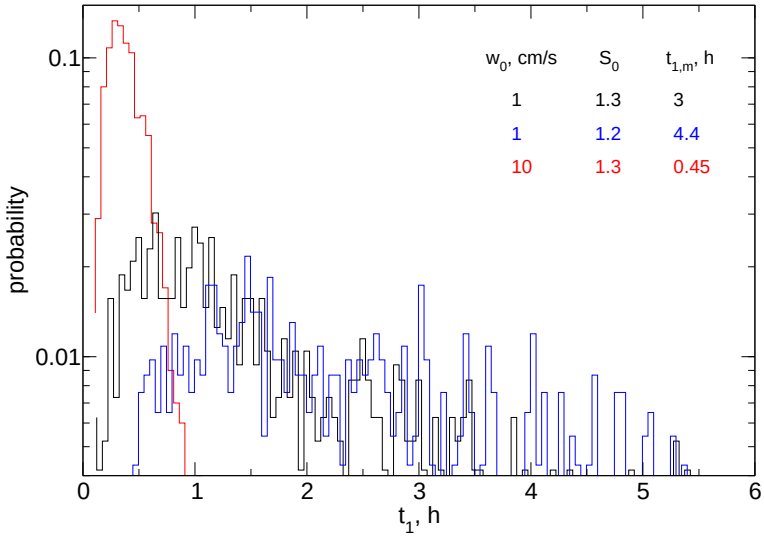

Figure S3. Probability distributions of first homogeneous freezing times in air parcels with an initial temperature about 3 K warmer than actual freezing temperatures. Constant updraft speed, w_0, and initial ice saturation ratio, S_0, are varied as indicated in the legend along with the mean freezing times, $t_{1,m}$ derived from the simulation data based on μ_w=10 cm s^{-1}.

Along each air parcel trajectory that is subject to random temperature fluctuations as described in section 2 in the main text, a certain time, t_1, elapses until homogeneous freezing conditions are reached for the first time. These conditions are formulated in terms of narrow ranges of the freezing temperature, $T_\star = 218 \pm 0.25$ K, and the associated ice saturation ratio, $S_\star = 1.5 \pm 0.02$. Clearly, t_1 depends on the initial values of these variables: $T_0 = 221$ K and $S_0 = 1.3$; t_1 also depends on the vertical wind speeds that are decomposed into a constant value, w_0, and fluctuating components, w' with a mean value μ_w=10 cm s^{-1}.

We extracted the times of first nucleation events from the ensemble simulations, and present their probability distributions in Fig. S3. Each distribution is based on 1,000 air parcel trajectories. For $w_0 = 1$ cm s^{-1} (black curve), the mean first freezing time is $t_{1,m} = 3$ h and the distribution is highly skewed containing very few individual data points well above 10 h (not shown). The distribution wing is controlled by the rare events in the vertical wind speed statistic. The broad peak region is centered around 1 h.

The fact that fluctuations are key in triggering freezing in the case $w_0 = 1$ cm s^{-1} is evident from the time required to increase S from S_0 to $S_\star$ in an air parcel cooling along the dry adi-

abate: $\tau \simeq 4\,\mathrm{h}$, exceeding $t_{1,m}$ by 1 h. Increasing w_0 tenfold shortens $t_{1,m}$ to 0.45 h, because then w_0 alone already accounts for the time to reach freezing conditions: $\tau(w_0) = 0.4\,\mathrm{h} \approx t_{1,m}$. In this case, which is closer to the deterministic regime, the fluctuations only slightly modify this time. The associated statistic (red curve) is therefore almost symmetric.

Slightly lowering S_0 by 0.1 increases $t_{1,m}$ by almost 50%, showing the strong sensitivity of freezing times on the initial relative humidity in the air parcel in the fluctuation-dominated regime. The peak region of the associated, flatter statistic (blue curve) shifts accordingly to the right by more than 30 min. However, this result will change if the forced temperature fluctuations are subject to damping not included in the model. Low frequency damping is required to obtain a stationary asymptotic temperature fluctuation variance across an ensemble of fluctuation time series in cases where the large-scale conditions are held constant. Therefore, it becomes increasingly unlikely to reach freezing thresholds in damped-driven simulations as initial conditions are chosen farther away from the actual freezing thresholds and the likelihood of late first freezing events occurring is reduced.